Alterations in metalloprotein abundance under ocean warming in the marine green alga *Micromonas pusilla* using the *mebipred* predictive tool

Craig J. Dedman [a,*], Marjorie Fournier [b], Rosalind E.M. Rickaby [a]

[a] *Department of Earth Sciences, University of Oxford, South Parks Rd, Oxford,OX1 3AN, United Kingdom of Great Britain and Northern Ireland*
[b] *Advanced Proteomics Facility, Department of Biochemistry, University of Oxford, South Parks Rd, Oxford OX1 3QU, United Kingdom of Great Britain and Northern Ireland*

A B S T R A C T

Metals are essential to life, required for the functioning of a substantial fraction of proteins. Marine phytoplankton drives the oceanic carbon cycle, influencing global biogeochemistry. These organisms rely on trace metal nutrients; however how trace nutrient demand will change under ocean warming is uncertain. The currently limited annotation of metalloproteins contributes to this lack of understanding. Herein, we utilise the recently published *mebipred* tool to predict the metalloproteome of the globally occurring green alga, *Micromonas pusilla*, revealing ~20 % of its reference proteome to display ion-binding properties. Using the predicted metalloproteome, and existing Gene Ontology annotation, we present a comprehensive insight towards changes in metalloprotein abundance after exposure to ocean warming conditions (+6 °C), using a shotgun proteomic approach. We outline that predictions must be combined with existing annotation to fully capture the metalloprotein response. Approximately 50 % of identified metalloproteins significantly altered in abundance under warming, largely related to changes in cellular function. Notably, warming appeared to shift Fe use from photosynthesis to storage in *M. pusilla*, indicated by a 2.36 log2 fold-increase in ferritin and decline in abundance of photosynthetic proteins. Ocean warming will inevitably alter cellular use and demand for metal cofactors in marine phytoplankton with possible implications for biogeochemical cycling. Bioinformatics tools such as *mebipred* greatly expand our ability to examine such changes.

1. Introduction

Growth of marine phytoplankton is limited by the availability of major (*i.e.,* nitrogen, phosphorous and silicon) and minor nutrients (*e.g.,* trace metals). Here, complex feedback relationships between nutrients and phytoplankton exist, which have influenced ocean biogeochemistry and evolution over millennia [1–3]. Metals are essential for life and it is predicted that >50 % of proteins require a metal cofactor for their correct function [4]. However, we are limited in our knowledge as only a minority of metalloproteins are known and fewer extensively characterised [5–7]. In phytoplankton, metals are key to fundamental physiological processes *i.e.,* photosynthetic carbon fixation, respiration, nitrogen fixation and defence against oxidative stress [1]. Some Metals, such as Mg, are in plentiful supply in seawater and therefore their role, primarily in photosynthesis, is not altered by their availability in the water column. However, trace metal nutrients whose bioavailability in the open ocean appears low compared to requirements for growth, limit

productivity of marine phytoplankton [1]. For example, Fe, which appears ubiquitously in the redox enzymes of photosynthesis and respiration, is estimated to limit growth in 30–40 % of the global ocean [1,8–10]. Thus, bioavailability of trace metals can impact upon phytoplankton community structure and productivity, in turn influencing biogeochemical processes such as the marine carbon cycle.

Ocean warming is the most direct impact of global climate change on the marine ecosystem [11]. Rates of physiological processes are largely dependent on enzymatic reactions, the kinetics of which are altered and generally increased at higher temperature [12]. As a consequence, phytoplankton metabolic rates (*i.e.* growth, photosynthesis and respiration) are recorded to rise with increasing temperature [13]. Due to the fact that trace metals are believed essential for the correct function of the majority of proteins, and given that they are known to play important roles in physiological processes that are rate-limited by temperature (*e.g.*, photosynthesis) [13,14], it is feasible to suggest that requirements for trace metals will alter under ocean warming. As the availability of trace

---

metal nutrients limits the growth of phytoplankton in the global ocean, any alteration to these requirements may incur added pressure on the phototrophic community, as well as impacting biogeochemical cycling. Whilst, we are gaining greater understanding on the impact of temperature on marine phytoplankton growth and physiology [13,15–17], to date, we have little knowledge on the impacts of temperature on the trace metal requirements and abundance of metal-binding proteins in phytoplankton. Never has this been more important to understand, given the imminent threat of climate change and the critical role marine microbial species play in major biogeochemical and climatic cycles.

One reason for our limited understanding of changing metalloprotein abundance in response to environmental variables is due to their limited characterisation, described above. This is particularly problematic in marine phytoplankton given that only a small selection of reference proteomes are currently available for eukaryotic species. Functional annotation of these reference proteomes is commonly limited, particularly in terms of metal-binding properties. Given this shortfall, efforts have been directed to generate effective tools which can be used to predict metal-binding properties of a protein of interest [7,18]. Recently, a new machine-learning based computational tool has emerged in the literature, *mebipred*, enabling ion-binding prediction to be made for a range of metal ions based on sequence data alone [7]. Using a homology-based approach, trained using metal-binding sequences derived from the Protein Data Bank (PDB) [19], *mebipred* identifies metal-binding sites without sequence alignment and does not require a high resolution structure, considerably reducing the time taken for analysis. *Mebipred* is reported to achieve an accuracy of >80 % and can be used to predict binding of whole protein sequences as well as fragments of peptides, opening up its scope for use with a range sequence-based data [7]. To utilise *mebipred*, sequence data must be uploaded to the server in FASTA format, as a result the tool allows the user to predict whole metalloproteomes by submitting the reference proteome of a particular species of interest. The resultant "reference metalloproteome" can subsequently be used to analyse shotgun proteomic data, facilitating the examination of metalloprotein abundance, and hence inference of changing demand for metal cofactors within the cell.

In this study we employ a novel technique combining use of shotgun proteomic analysis and *mebipred* ion-binding prediction to examine alterations in cellular function and abundance of metal-binding proteins in the globally occurring green alga, *Micromonas pusilla*, proposed as an effective model for ocean warming research [20,21]. Analysis of the *M. pusilla* metalloproteome using the *mebipred* tool, revealed a previously uncharacterised set of metalloproteins, enhancing our functional annotation of its reference proteome. In response to ocean warming, *M. pusilla* appeared to significantly alter cellular function but not growth, associated with a significant alteration in abundance of ~50 % of identified metalloproteins.

2. Methods

2.1. mebipred metal-binding prediction

The *mebipred* server was accessed using services.bromberglab.org /mebipred and the reference proteome UP000001876 (*Micromonas pusilla* CCMP1545; downloaded 21/02/22) was submitted for metal-binding prediction using the default settings. The metal-binding prediction follows a two-tiered approach; first (tier 1), prediction of whether a sequence displays metal-binding and, second (tier 2), prediction of the specific ion (Ca, Co, Cu, Fe, K, Mg, Mn, Na, Ni or Zn). For each of the metal-binding predictions a score is generated by *mebipred* in the range 0–1. To identify metal-binding proteins, we followed recommendations outlined by the developers of *mebipred* [7]. A cut-off of 0.5 was utilised in the first tier of analysis, whereby those proteins with a tier 1 score of >0.5 were classified as metal binding. For these proteins, associated ions were identified where their score was >0.5. In cases

where the tier 1 score was <0.5, but the ion score in tier 2 was >0.5, the cut-off value for the tier 2 score was increased to >0.9, believed to accurately predict metal-binding properties [7]. To examine the function of predicted proteins, enrichment analysis was carried out on groups of metal-binding proteins (*e.g.,* Fe-binding proteins) using the online DAVID platform [22,23].

2.2. Experimental conditions

Micromonas pusilla RCC1614 culture was acquired from the Roscoff Culture Collection (France) and transferred to filter-sterilised (0.22 μm) F/2 + Si media [24]. Cultures were held in 50 mL filter-capped tissue culture flasks and placed in PHCbi MLR-352-PE Incubators (PHC Europe B.V.) set at 17 °C (control) or 23 °C (warming), under a lighting regime of 14:10 h light:dark and a light intensity of 30–50 μmol m^{-2} s^{-1}. A total of three biological replicates were examined per treatment. *M. pusilla* was additionally grown at an extreme warming treatment of 28 °C; however no growth was recorded in this condition. Growth of *M. pusilla* was monitored daily by means of chlorophyll fluorescence and optical density at 750 nm (OD750) using a Tecan Spark plate reader. Briefly, a 200 μL sub-sample was taken and three technical replicates measured for each sample. Specific growth rates (μ) were calculated based on values obtained for chlorophyll fluorescence and OD750, respectively. Cultures were transferred to new media upon reaching mid-exponential growth and exposed to experimental conditions for a period of six weeks. During the final transfer, the culture volume was increased to 200 mL for harvesting of cell material for shotgun proteomic analysis, no effect of the increase in culture volume on growth was recorded. Here, upon reaching mid-exponential growth, determined to be day 7 of growth (Fig. SI.1), cells were harvested by centrifugation at 3000 rpm (10 min) at 4 °C. Cell pellets were immediately placed at −80 °C.

2.3. Proteomic analysis

Cell pellets harvested during mid-exponential growth were thawed at room temperature and resuspended in extraction buffer (20 mM Tris-HCl, pH 8.0). Using a sonication bath, cells were lysed by three rounds of sonication on ice for a period of 10 min. Protein concentrations were determined using a Bradford assay [25]. In-solution trypsin digestion was subsequently carried out on 100 μg protein per sample. Cysteines were reduced using 10 mM tris(2-carboxyethyl)phosphine (TCEP) and alkylated with 50 mM iodoacetamide. Proteins were digested using LysC before the trypsin reaction was carried out. Digested proteins were desalted using C18 stage-tips prior to LC-MS/MS analysis. Peptides were separated by nano liquid chromatography (Thermo Scientific Ultimate RSLC 3000) coupled in line a Q Exactive mass spectrometer equipped with an Easy-Spray source (Thermo Fischer Scientific). Peptides were trapped onto a C18 PepMac100 precolumn (300 μm i.d.x5mm, 100 Å, ThermoFischer Scientific) using Solvent A (0.1 % Formic acid, HPLC grade water). The peptides were further separated onto an Easy-Spray RSLC C18 column (75um i.d., 50 cm length, Thermo Fischer Scientific) using a 60 min linear gradient (15 % to 35 % solvent B (0.1 % formic acid in acetonitrile)) at a flow rate 200 nL/min. The raw data were acquired on the mass spectrometer in a data-dependent acquisition mode (DDA). Full-scan MS spectra were acquired in the Orbitrap (Scan range 350-1500 *m/z*, resolution 70,000; AGC target, 3e6, maximum injection time, 50 ms). The 10 most intense peaks were selected for higher-energy collision dissociation (HCD) fragmentation at 30 % of normalized collision energy. HCD spectra were acquired in the Orbitrap at resolution 17,500, AGC target 5e4, maximum injection time 120 ms with fixed mass at 180 *m/z*. Charge exclusion was selected for unassigned and 1+ ions. The dynamic exclusion was set to 20 s. Raw data were analysed for label-free quantification (LFQ) and proteins identified using MaxQuant v2.0.3.0 [26], in-line with the *M. pusilla* reference proteome (UP000001876). The MaxLFQ workflow was used to determine normalized LFQ values for each protein identified during analysis [27].

Downstream analysis was conducted using Perseus v1.6.15.0 [28]. Alterations in protein abundance (LFQ intensity) were examined by use of FDR-corrected two-way *t*-tests between the 17 °C control and 23 °C warming treatment (q ≤ 0.05), generating log2 fold-change values. To consider alterations in metal-binding and functional protein groups, LFQ values were converted to relative abundance by normalising to peptide length [29]. Alterations in cell function were examined using enrichment analysis of significant proteins using the online DAVID platform [22,23]. Metal-binding proteins were identified using the predicted metalloproteome obtained using *mebipred* as well as existing Gene Ontology annotation (see Supplementary information Section SI.1) [30]. The mass spectrometry proteomics data have been deposited to the ProteomeXchange Consortium *via* the PRIDE partner repository with the dataset identifier PXD038244 [31].

3. Results & discussion

3.1. Predicting the M. pusilla metalloproteome utilising the mebipred tool

The full reference proteome available for *M. pusilla* (10,250 protein sequences) was submitted to the *mebipred* server for prediction of metal-binding properties. This tool uses a two-tiered approach, described above, to predict metal-binding properties of protein sequences. Predictions are made regardless of the oxidation state or context of the ion of interest, hence Fe^{2+}, Fe^{3+} and heme are all represented by the Fe-binding category [7]. Utilising recommended thresholds (see Methods), 1419 proteins were identified to meet the criteria for tier 1 and a further 571 proteins which met the criteria for tier 2, representing 19.4 % of the reference proteome of *M. pusilla* (Supplementary data Table 1). The proportion of the reference proteome predicted to bind each respective ion is presented in Fig. 1A. Proteins predicted to bind to Zn represented the largest ion-binding group identified, representing 8.2 % of proteins in the reference proteome, following by K-binding (7.0 %) and Ca-binding (5.7 %) proteins, respectively. All remaining groups represented ~2–4 % of the reference proteome. Approximately 40 % of the ion-binding proteins identified were predicted to associate with a single ion (Fig. 1B), although this varied greatly. For example, ~50 % of Cu-binding proteins were predicted to bind Cu only, whereas just ~4 % of Mg-binding proteins were predicted to only bind Mg. As expected given their stringent selection criteria, those proteins derived from tier 2 of the *mebipred* analysis were less commonly associated with >1 ion.

To gain insight towards the effectiveness of *mebipred,* we compared

metal-binding predictions with current annotation, focussing on the comprehensive and widely used Gene Ontology (GO) knowledgebase [30]. Of the 10,250 proteins in the *M. pusilla* reference proteome, 5964 are currently annotated with GO terms. Identification of metalloproteins based on GO annotation alone revealed a total of 930 proteins (~9 % of the reference proteome) (for a full list of GO terms used see Section SI.1. Supplementary information), approximately half the number identified using *mebipred*. The greater identification of metalloproteins by *mebipred* is expected given that those proteins for which no annotation currently exists can be included in analysis. It is acknowledged by the developers of *mebipred* that predictions are not always consistent with current functional annotations [7]. In-line with this we identified a number of inconsistencies between current GO annotation and *mebipred* predictions. Of the 930 proteins which possessed metal-related GO annotation, 355 (38 %) were identified as metal-binding by *mebipred*. The remaining 575 did not meet predicted metal-binding thresholds but included some well-characterised metalloproteins critical to phytoplankton cellular function, for example RuBisCO, ferredoxin, magnesium chelatase and a number of metal ion transport and storage proteins. Of the 355 proteins which are described as metal-binding by both methods, 112 were predicted by *mebipred* to bind the same ion as referred to in GO terms. However, *mebipred* revealed that in 75 cases, the protein was predicted to interact with additional ionic species. For 82 proteins, there was disagreement between GO terms and *mebipred* prediction of the interacting ion. Over one third of the proteins annotated with metal-related GO terms did not contain any information regarding the specific metal ion. In this manner *mebipred* was able to provide new insight to the likely ion-binding activity of 159 proteins for which annotation currently exists.

Whilst >50 % of proteins are predicted to associate with a metal cofactor [4], we are currently limited in our knowledge of the metal-binding properties of a large proportion of proteins and hence are unable to examine those functions most impacted by metal cofactor availability. To gain insight towards the function of specific ion-binding groups identified using *mebipred*, protein lists predicted to bind each ion were submitted for functional enrichment analysis *via* the DAVID server (Sections SI.2, Supplementary information and Supplementary data Table 2) [22,23]. Notably, we found a considerable overlap between functional features belonging to each ion-binding group. In particular, enriched terms identified in the Zn-binding protein group appeared common across a number of metals. Largely, functions were related to processes known to be associated with each ion of interest, providing
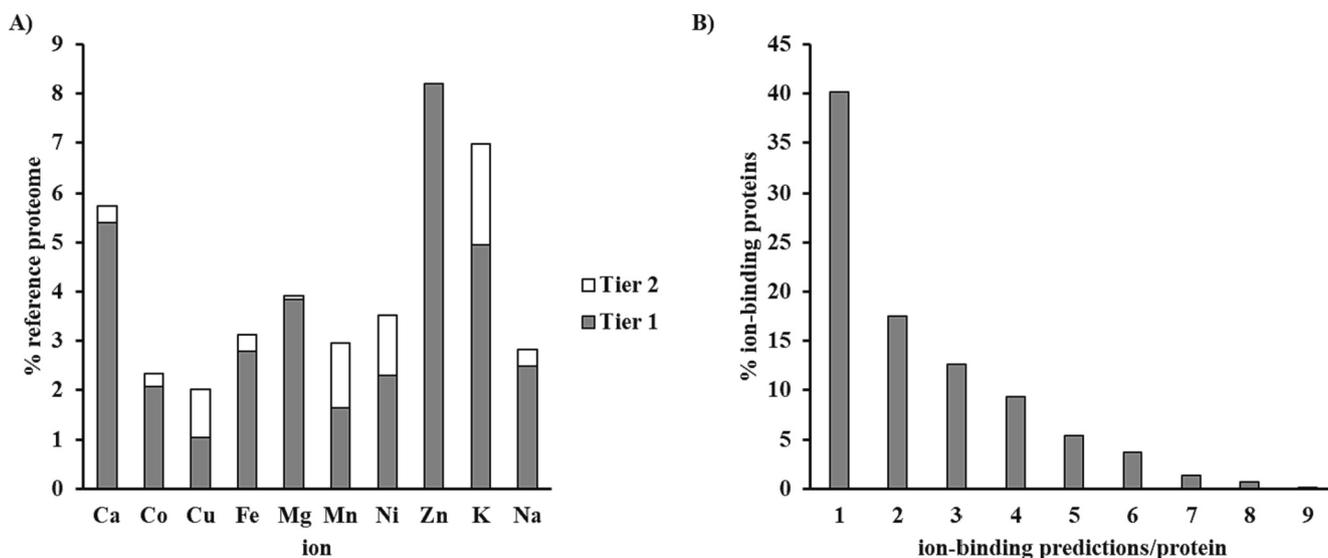

Fig. 1. *Mebipred* prediction of ion-binding properties of the *M. pusilla* proteome. Panel A displays the proportion of the reference proteome predicted to bind to each ion type, respectively. Panel B displays the number of ionic species predicted to bind to each individual protein.

confidence in their identification as metal-binding by *mebipred*. We acknowledge that such analyses are biased towards those proteins for which annotation exists. Approximately, one third (37 %) of metalloproteins identified by *mebipred* had no existing GO annotation.

It is clear given the current lack of metalloprotein characterisation that new methods are required to facilitate our understanding of the role of metalloproteins in organismal function and their environmental response. The *mebipred* tool greatly expands the current annotation of the *M. pusilla* metalloproteome, and through functional enrichment analysis we are able to improve our understanding of possible metalloprotein function. An advantage of *mebipred* is the ability to consider that multiple ionic species may interact with a particular metalloprotein, information which will be of great utility when considering impacts of altering trace nutrient abundance or metal toxicity. In future it will be important to validate binding predictions, as well as relative affinities for each ion. However, caution must be taken when using such tools given the lack of identification of key metalloproteins (*e.g.*, RuBisCO) and inconsistencies between metal-binding predictions and current annotation such as GO described above.

3.2. Growth of M. pusilla and impact of ocean warming on the cellular proteome

To examine the impact of ocean warming on metalloprotein abundance in *M. pusilla*, cultures were harvested for shotgun proteomic analysis during mid-exponential growth following a six-week exposure to a 6 °C increase in temperature. After filtering of data and removal of potential contaminants, a total of 1735 proteins were utilised for downstream analysis and inference of altering abundance of metalloproteins in *M. pusilla* under warming (Supplementary data Table 3). Statistical analysis by means of FDR corrected two-way *t*-tests (q ≤ 0.05), revealed that warming caused a significant alteration in abundance of 43 % of the identified proteome (Fig. 2), with an equal number of proteins being relatively more or and less abundant in the warmed 23 °C treatment compared to the 17 °C control (q ≤ 0.05). This significant alteration in cellular function is expected given the known impacts of temperature upon phytoplankton metabolism [12,13,15]. Temperature has previously been shown to influence growth of various members of the *Micromonas* genus in a strain-specific manner, largely in-line with their geographical origin [21]. Despite the significant alterations in the identified proteome recorded, increasing temperature from 17 °C to 23 °C had negligible impact on growth of *M. pusilla* in this study (Table 1). In previous work, *M. pusilla* has been shown to display a greater variation in its thermal response than other members of the *Micromonas* genus, occupying a thermal niche of 28.9 ± 5.3 °C [21]. This work identified the optimal temperature of *M. pusilla* to be in the range 22–24 °C [21], however other work reports this value as high as 28.7 °C [15], highlighting the variation in such measures that exists between studies. Given these values, in our work we would expect *M. pusilla* RCC1614 to display improved growth in the warmed treatment, as 23 °C lies within the optimal thermal range previously reported [21]. In both of these previous studies, direct cell counts *via* flow cytometry were used to determine rates of growth. It is possible that the plate reader measurements utilised in our study are not as accurate in revealing alterations in growth rate of *Micromonas*. Alternatively, it is possible given the high variability in thermal response displayed by various *M. pusilla* strains [21], that RCC1614 used in our study may occupy a slightly different thermal niche to those previously examined. This strain was isolated from the North Sea at a higher latitude (57°) than those strains examined previously (41.5–50.5°), and in our work was unable to grow at 28 °C, within the thermal niche reported for *M. pusilla* by Demory *et al* (2019) and close to the optimal temperature reported by Barton et al. (2019). The optimal temperature for RCC1614 may lie between 23 °C and 28 °C, however further work is required to confirm this. Additional measures to explore alterations in cell number, cell size and biochemistry would be beneficial to fully delineate the

thermal response of RCC1614, however this was beyond the scope of the present study.

Significant proteins were submitted for functional enrichment analysis using the DAVID server [22,23], revealing key insight into the cellular functions most impacted by temperature in *M. pusilla* (Supplementary data Table 4). First, in-line with work on the coccolithophore *E. huxleyi*, and previous works examining the response of marine phytoplankton to temperature, translation appeared to be down-regulated within the warmed treatment (Fig. 2) [12,32,33]. Within the identified proteome, 99 proteins were annotated with the GO Term "translation", representing on average 17.5 % of the proteome in cultures grown at 17 °C, decreasing to 13.9 % at 23 °C. A total of 69 of these proteins were significantly less abundant at 23 °C compared to 17 °C (q ≤ 0.05). This decline in translation suggests a decrease in ribosomal content under ocean warming, supported by significant decreases in ribosome biogenesis and assembly proteins (C1N7U3 and C1MYK7; q ≤ 0.05). Decreases in ribosomal investment under warming are suggested to result from an increase in translation efficiency at higher temperature, resulting in increased rates of protein synthesis from reduced ribosomal content [12]. Accordingly, whilst ribosomal content appeared down-regulated in our study, terms relating to protein transport were enhanced under warming, suggesting an increase in protein synthesis in the warmed treatment. However, this was not associated with an increase in cell growth. The relative decrease in P-rich ribosomal content and rise in N-rich proteins, will likely increase N:P ratios under ocean warming with consequences for nutrient cycling [12]. On the one hand, the decline in P demand, may mitigate impacts of nutrient stratification associated with ocean warming [34]. Conversely, increasing rates of protein synthesis associated with increased cellular N:P ratios may drive increased N demand [12], placing strain on this element which already limits phytoplankton growth in the ocean [35]. Any alteration in the elemental stoichiometry of phytoplankton will likely impact grazers such as zooplankton due to changes in nutritional quality. Typically, the C content of phytoplankton exceeds that required by zooplankton, whilst N and P is limited [36]. Should improvements to translation efficiency drive increased N:P, this will likely have a mixed impact on zooplankton by improving access to N while decreasing P supply. However, Kwiatkowski et al. (2018) predict an overall decline in phytoplankton nutritional quality during the 21st century, with greatest declines in C:N and C:P content observed in the Arctic ocean, where *Micromonas* dominates the picophytoplankton assemblage [36,37]. Further investigation on the likely impact of warming on the stoichiometry of this ecologically important genus is required to accurately predict the likely biogeochemical and trophic impact on this key ecosystem.

A total of 17 proteins associated with protein transport were significantly increased in the warmed treatment (q ≤ 0.05) (Fig. 2). Greatest change was seen in abundance of a type II secretary family protein (C1MX36) which displayed a 1.22 FC increase (q ≤ 0.05). Whilst protein transport was identified by functional enrichment analysis to be enriched in proteins which displayed significantly increased abundance under warming, proteins relating to protein folding appeared to display an opposite trend (Fig. 3). Here, 15 proteins associated with protein folding displayed a significant decline in the warmed treatment. A number of these proteins were subunits of the highly-conserved CCT complex, responsible for the mediation of protein folding in eukaryotic species [38], displaying a − 0.29 to −0.73 FC decrease (q ≤ 0.05). The most abundant peptidyl-prolyl cis-trans isomerase (PPIase; C1N203), likely playing a role in protein processing [39], was also recorded to decrease −0.77 FC (q ≤ 0.05). Another feature identified to be enriched in proteins more abundant under warming was the presence of a calcium ion binding domain. These proteins were associated with a range of functions including, cell signalling, protein folding and photosynthesis.

The most abundant proteins identified during analysis were histones and associated proteins, representing 26–33 % of the identified proteome. On average these proteins increased in abundance under warming,
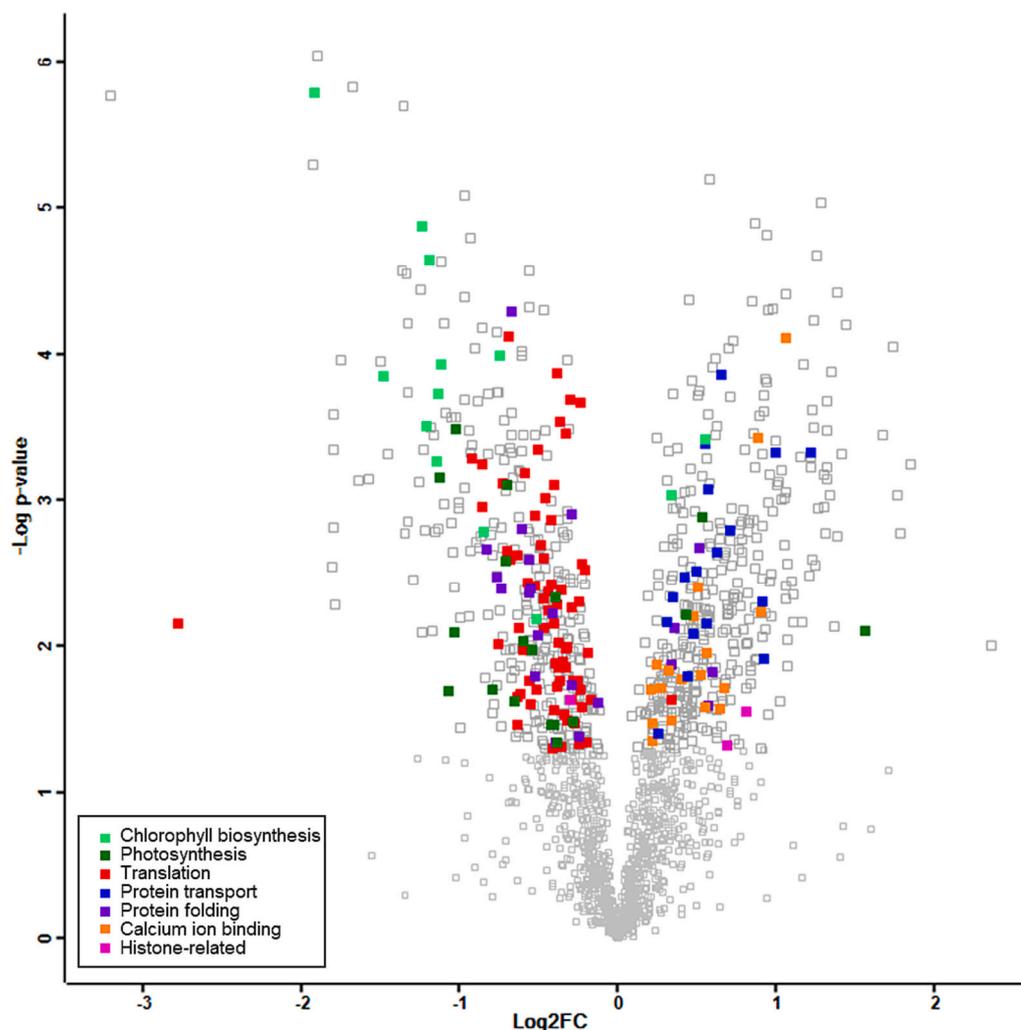
Fig. 2. Volcano plot displaying significantly altered proteins (large symbols) in *M. pusilla* acclimated to ocean warming (23 °C) relative to the control (17 °C) (n = 3; q ≤ 0.05). Coloured symbols display key changes in protein functions under the warming treatment.

Table 1
Growth of *M. pusilla* under warming.

	Specific growth rate (μ)	
	Chlorophyll	OD750
17 °C	0.56 ± 0.03	0.20 ± 0.03
23 °C	0.55 ± 0.01	0.22 ± 0.03

Data is presented as the mean ± standard deviation (n = 3).

driven by a significant 0.81 FC in abundance of histone H4 (C1MUM2) from 5.02 % to 8.47 % (q ≤ 0.05). The genome of eukaryotic organisms is packaged into chromatin, made of up histones and DNA in the form of nucleosomes [40]. The nucleosome is typically ~150 bp of DNA which wraps around a histone octamer formed of pairs of H2A, H2B, H3 and H4 [41,42]. Organisms are able to modify properties of the nucleosome by means of histone variant replacement, post-translational modification and movement of the histone core, in doing so controlling chromatin-based gene regulation [43]. It is proposed that alteration of the nucleosome, such as the increase in histone H4 observed in *M. pusilla* under warming, may influence its stability and ability to slide along or be detached from DNA, thus regulating DNA exposure [43]. Such a process may be a part of the genetic regulation of the warming response in *M. pusilla* and requires further investigation.

A key alteration of the proteome revealed by enrichment analysis,

was a decline of chlorophyll biosynthesis and photosynthetic machinery in the warmed treatment (Fig. 2). Ten proteins involved in chlorophyll biosynthesis were significantly reduced (−0.85 to −1.92 FC) in the warmed treatment compared to 17 °C (q ≤ 0.05). Here, greatest change was seen in abundance of magnesium chelatase (C1MQ15), the rate limiting step of chlorophyll generation [44]. Chlorophyll biosynthesis has previously been recorded to decline in both coccolithophore and diatom species in response to increasing temperature [33,45,46]. This highlights a key consideration of the accuracy of using chlorophyll-based measures of growth and abundance in warming experiments, a factor which may have contributed to the lack of alteration in growth rate of *M. pusilla*, described above, whereby a declining chlorophyll per cell may have masked an increase in growth rate. Alongside the reduction in chlorophyll biosynthesis, *M. pusilla* cultures in the warmed treatment also displayed a lower abundance of photosystem I (PSI) and photosystem II (PSII) proteins. Of the 9 PSI proteins identified, 8 were found to be significantly less abundant under warming (−0.28 to −0.65 FC; q ≤ 0.05), with relative abundance of PSI proteins reducing from 1.89 ± 0.06 % to 1.53 ± 0.14 %. Similarly, 5 of the 7 PSII proteins identified were on average less abundant in the warmed treatment, significant for 3 (−0.69 to −1.13 FC; q ≤ 0.05). Each of these proteins were associated with the oxygen-evolving complex of PSII, which is known to become unstable in response to elevated temperature [47]. Accordingly, abundance of the PSII stability/assembly factor (C1MMU8) was significantly increased under warming (0.65 FC; q ≤ 0.05). In total,
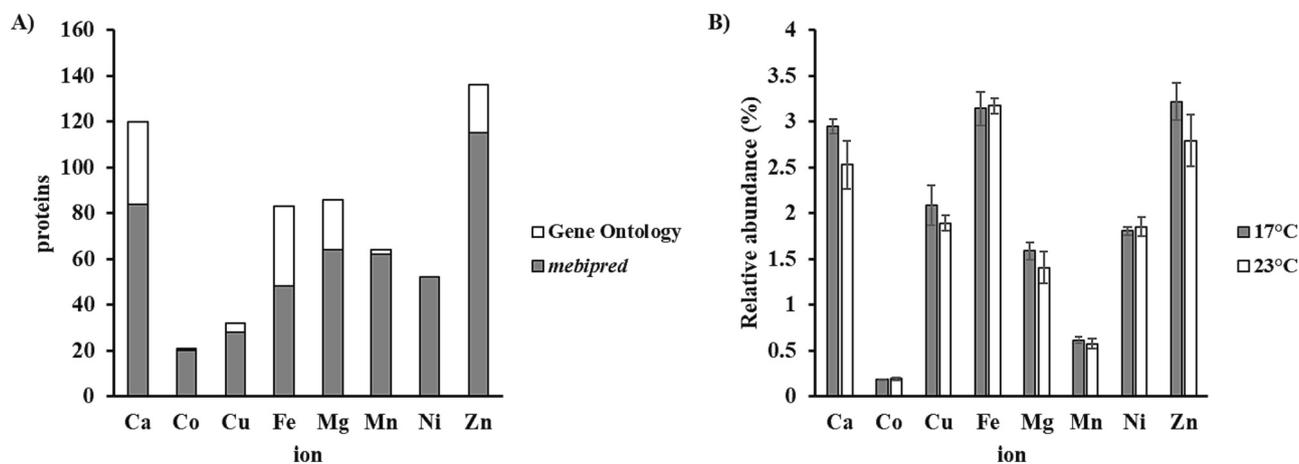
Fig. 3. Metalloproteins identified during proteomic analysis of *M. pusilla* (A) and relative abundance of respective metal-binding groups (B). Relative abundance data is presented as the mean ± standard deviation ($n = 3$).
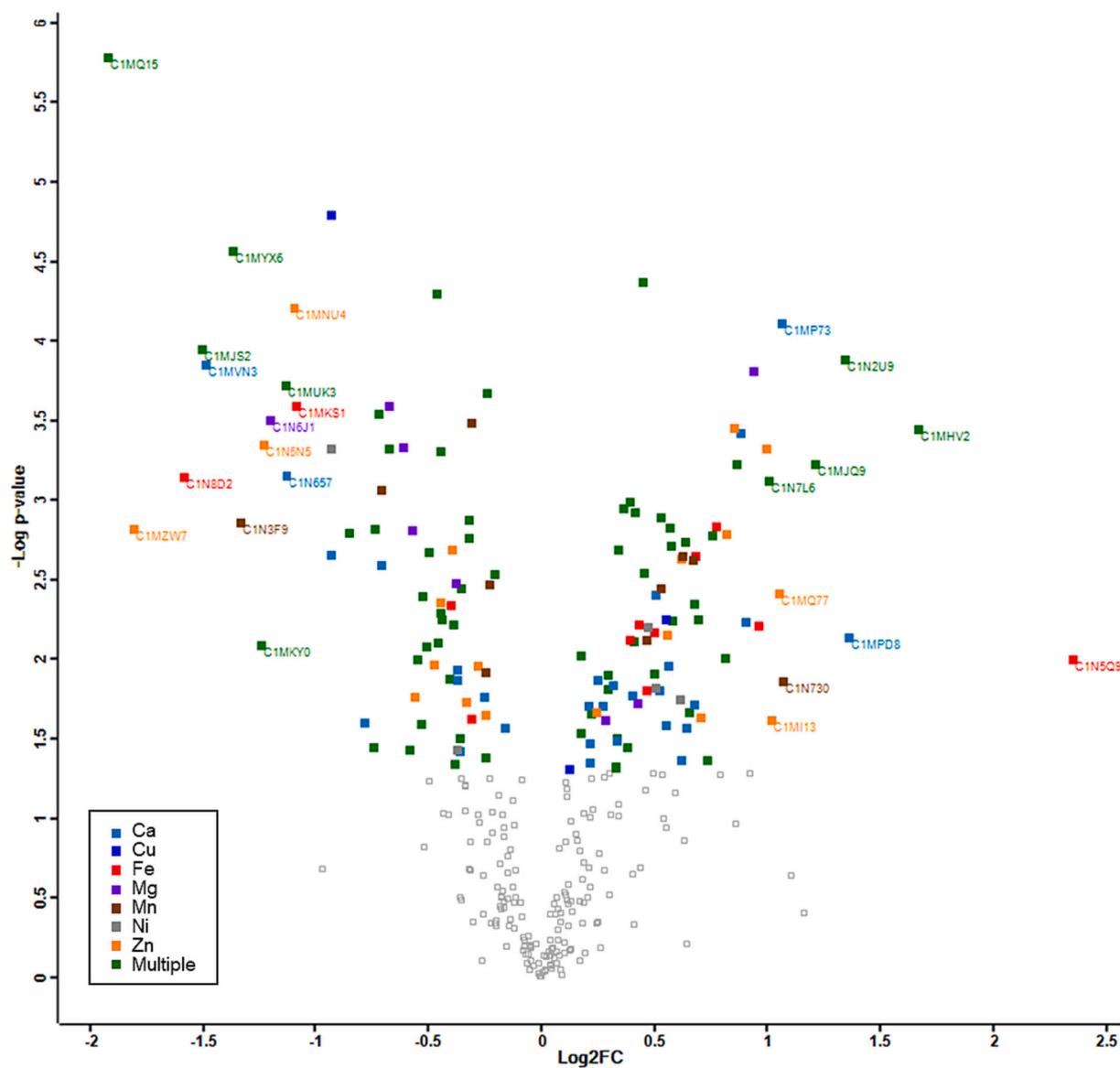

Fig. 4. Volcano plot displaying significantly altered metalloproteins (coloured symbols) in *M. pusilla* acclimated to ocean warming (23 °C) relative to the control (17 °C) ($n = 3$; q ≤ 0.05). The binding ion is indicated by symbol colour, as displayed in the legend. Protein IDs are provided for those proteins displaying a log2FC of >1, listed in Table 2.

relative abundance of PSII proteins decreased to a greater extent than PSI, reducing from $2.65 \pm 0.09\%$ to $1.62 \pm 0.16\%$. Correspondingly, on average the cross-sectional area of PSII was consistently recorded to be lower at 23 °C compared to 17 °C (Fig. SI.2B, Section SI.4). Despite these changes, measures of photosynthetic efficiency (Fv/Fm) (Fig. SI.2A, Section SI.4), revealed little impact of these cellular alterations upon photosynthetic performance. The lack of improvement in photosynthetic performance of *M. pusilla* in the range 17–23 °C is in disagreement with previous research which reports that peak photosynthetic rates are achieved at temperatures of ~25 °C for this species [13]. The reduction in relative abundance of photosynthetic proteins suggests a lowered cost of photosynthesis as temperature rises, as previously described [33,48], supported by a maintenance of Fv/fm whilst PSII appeared down-regulated. It remains unclear as to why this reduction in photosynthetic investment in the warmed condition did not correspond to an increase in growth of *M. pusilla,* but supports the likelihood of *M. pusilla* RCC1614 occupying a separate thermal niche to those strains previously examined.

3.3. Alterations in abundance of metalloproteins after acclimation to warming

The data obtained from shotgun proteomic analysis of *M. pusilla* cultures was mapped to the predicted metalloproteome generated using *mebipred*, identifying 270 predicted metal-binding proteins, representing ~16 % of the identified proteome. As discussed in Section 3.1, inconsistency exists between *mebipred* and current GO annotation. Hence to account for this, we additionally used GO annotation to identify metal-binding proteins which were not identified by the *mebipred* tool for each metal ion investigated in this study (Ca, Co, Cu, Fe, Mg, Mn, Ni and Zn). A further 122 metal-binding proteins were identified for analysis using this method (Fig. 3A).

To examine alterations in abundance of various metal-binding protein groups, LFQ values were converted to relative abundance values (%) and relative abundance of proteins predicted/annotated to bind to each ion was calculated. Here, it is accepted that proteins are likely to bind more than one ion type, hence further work would be required to confirm the exact metal ion bound and thus any altering nutrient

demand inferred from this analysis. Upon examining changes in protein abundance at the ion- level (*e.g.*, Fe-binding proteins), little variation was seen between warmed and control cultures (Fig. 3B). Despite this, in-line with the considerable impact of warming on the cellular proteome of *M. pusilla* described above, a substantial fraction of the metal-binding proteins identified (47 %) displayed significantly altered abundance under warming (q ≤ 0.05) (Fig. 4), contributing to the overall alterations in cellular function observed. The vast majority of these proteins were predicted to interact with more than one metal ion (Fig. 4). A total of 24 metal-binding proteins were recorded to display a >1 FC in the warming treatment (Fig. 4 and Table 2).

3.3.1. Iron

Fe is essential to phytoplankton growth. Eighty-three Fe-binding proteins were identified during proteomic analysis, of which 32 displayed significantly altered abundance under warming (q ≤ 0.05) (Supplementary data Table 3). Whilst the abundance of individual Fe-binding proteins varied significantly, little difference in the total relative abundance of Fe-binding proteins was observed (Fig. 3B). The greatest alteration observed through proteomic analysis was that of ferritin (C1N5Q9), which appeared significantly raised 2.36 FC in the warmed condition (q ≤ 0.05) (Fig. 4; Table 2). Whilst representing the primary Fe-storage protein in eukaryotic phytoplankton [49], this protein was not identified as Fe-binding by *mebipred*, but instead was identified using GO annotation, again highlighting the need to utilise existing annotation alongside metal-binding prediction tools. It is not clear as to why such an increase in ferritin was observed in the warmed treatment, however this may be related to the reduction in abundance of photosynthetic proteins, which represent a significant Fe cost, freeing up Fe which could then be stored. Such an increase in ferritin abundance may result in an increase in the cellular Fe pool, thus raising the Fe content of phytoplankton. Alongside increases in ferritin abundance, ferrochelatase (C1N107), which catalyses the production of heme [50], was significantly raised in cultures exposed to warming (0.96 FC; q ≤ 0.05). Similarly, the cytosolic Fe—S cluster assembly factor NBP35 (C1MLK8), also displayed a significant increase (0.47 FC; q ≤ 0.05). Like ferritin, NBP35 was also not identified by mebipred as Fe-binding. In-line with this, the heme-containing cytochrome *b*5-like protein

Table 2
Significant metal-binding proteins displaying a fold-change of >1 (Log2FC) under warming.

	Relative LFQ intensity						Log2FC	Ion(s)	Identification
	17°C	17°C	17°C	23°C	23°C	23°C			
C1N5Q9| Ferritin							**2.36**	Fe	GO
C1MHV2| Predicted protein							**1.67**	Mn; Cu; Zn; Co	MebiPred
C1MPD8| Calcium-transporting ATPase							**1.36**	Ca	GO
C1N2U9| Predicted protein							**1.35**	Ni; Zn; Mg	MebiPred
C1MJQ9| Predicted protein							**1.22**	Fe; Ni; Zn	MebiPred
C1N730| D-fructose-1,6-bisphosphate 1-phosphohydrolase							**1.07**	Mn	MebiPred
C1MP73| Diphthamide synthase							**1.06**	Ca	GO
C1MQ77| Predicted protein							**1.06**	Zn	GO
C1MI13| Protein-serine/threonine kinase							**1.02**	Zn	MebiPred
C1N7L6| Predicted protein							**1.01**	Ca; Mn	MebiPred
C1MKS1| 3-isopropylmalate dehydratase							**-1.08**	Fe	GO
C1MNU4| Adenosylhomocysteinase							**-1.10**	Zn	MebiPred
C1N657| Oxygen-evolving enhancer protein 3							**-1.13**	Ca	GO
C1MUK3| Mg-protoporphyrin IX chelatase							**-1.13**	Ni; Mg	Both
C1N6J1| Mg-protoporphyrin IX monomethyl ester cyclase							**-1.20**	Mg	GO
C1N6N5| Predicted protein							**-1.23**	Zn	MebiPred
C1MKY0| Predicted protein							**-1.24**	Ca; Zn	MebiPred
C1N3F9| Light induced like protein							**1.33**	Mn	MebiPred
C1MYX6| Pyruvate kinase							**-1.37**	Mn; Mg	Both
C1MVN3| Predicted protein							**-1.49**	Ca	MebiPred
C1MJS2| Calcineurin-like phosphoesterase							**-1.51**	Zn; Ni	MebiPred
C1N8D2| Quinolinate synthase							**-1.58**	Fe	GO
C1MZW7| Predicted protein							**-1.80**	Zn	Both
C1MQ15| Mg chelatase							**-1.92**	Ca; Mg; Zn	Both

Relative LFQ intensities for each biological replicate (n=3, per treatment; q≤0.05) are represented by a blue to red colorimetric scale.

(C1MGX5) and Fe-S-containing NADH nitrate reductase (C1MRK2) displayed a 0.68 FC and 0.42 FC increase under warming ($p \leq 0.05$). These results suggest enhanced production of Fe- cofactors in the warmed treatment, which may additionally increase the cellular Fe quota. However, given the decline in photosynthetic proteins, which constitute a major Fe pool, this may mitigate any impact of increased Fe storage or cofactor production. Further work is required to confirm any alteration to cellular Fe content.

Fe plays an important role in electron transport systems of both photosynthesis and respiration. The most abundant Fe-protein identified was Ferredoxin (C1N7Q8), representing ~1 % of the identified proteome. This ferredoxin did not show any alteration in abundance under warming and was not predicted to be metal-binding by *mebipred*. However, ferredoxin NADP reductase (FNR; C1N984) displayed a significant decline in abundance at 23 °C compared to 17 °C (−0.40 FC; q ≤ 0.05). FNR catalyses the final step of photosynthetic ATP production. Conversely, ferredoxin thioredoxin reductase (FTR; C1MYV2) was significantly raised 0.43 FC under warming (q ≤ 0.05). FTR is reported to play a key role in modulating carbon fixation in photosynthetic organisms by regulating the Calvin cycle and Pentose phosphate pathways [51]. Related to this several components of carbon metabolism were significantly altered under warming. For example, the Fe-binding 3-isopropylmalate dehydratase (C1MKS1), homologous to aconitase, and isocitrate dehydrogenase (C1N5W5) which both function in the tricarboxylic acid cycle displayed a − 1.08 FC decline and 0.78 FC increase in response to warming, respectively (q ≤ 0.05). The Fe-binding protein which displayed the greatest reduction in abundance under warming was quinolinate synthase (C1N8D2) (−1.58 FC; q ≤ 0.05) (Fig. 4; Table 2). This enzyme acts to produce nicotinamide adenine dinucleotide (NAD), a key cofactor in a variety of redox reactions [52].

3.3.2. Calcium

Ca plays an important role in a number of cellular processes including, cell signalling and protein processing [53]. Ca-binding was identified as a significant feature of proteins which were significantly increased in abundance under warming during enrichment analysis (Supplementary data Table 4), however the relative abundance of Ca-proteins was observed to decline on average from 2.9 % to 2.5 % under warming ($p = 0.06$). A total of 120 proteins were identified to bind *Ca*. Approximately, one quarter of these proteins were identified based on GO terms only. Sixty-five Ca-binding proteins were recorded to display altered abundance under warming, 39 of which significantly increased in abundance (q ≤ 0.05) (Supplementary data Table 3). While Ca-proteins displayed an average decline, the Ca-transporting ATPase (C1MPD8) was significantly raised 1.36 FC in the warmed treatment (q ≤ 0.05), suggesting an increase in Ca uptake/transport within the cell. An increase in cellular Ca content is supported by increased abundance of calreticulin (C1N041; 0.50 FC; q ≤ 0.05), a protein which plays multiple roles including regulating Ca-homeostasis and protein processing [54], and calmodulin (C1ML90; 0.70 FC; q ≤ 0.05), the primary eukaryotic Ca^{2+} receptor [55]. The influx of Ca^{2+} and increase of calmodulin may represent an increase in cell signalling activity as *M. pusilla* responds to a warmed environment.

Ca also plays an important role in the water-splitting reaction of photosynthesis [56]. This reaction occurs in the OEC of PSII which based on protein abundance appeared to be down-regulated under warming. Three of the proteins involved in the response of the OEC to increasing temperature, are annotated by GO to be Ca-binding; the PSII manganese-stabilizing polypeptide (PsbO; C1N779), the PSII OEC 23 kDa protein (PsbP; C1MWZ0) and the oxygen-evolving enhancer protein 3 (PsbQ; C1N657), each significantly reduced −0.69 FC to −1.13 FC in the warmed treatment (q ≤ 0.05). None of these proteins were predicted to bind Ca using the *mebipred* tool. As mentioned above it is unclear given these significant changes to photosynthetic machinery why no alteration in efficiency of PSII was recorded between the two treatments. It is possible that photosynthetic performance is maintained at the higher temperature due to increasing rates of electron transport and light capture efficiency at the higher temperature [48], requiring less investment in photosynthetic apparatus. However, any energetic benefit to the cell as a result of this does not appear to translate into improved growth in *M. pusilla* RCC1614.

3.3.3. Zinc

In-line with *mebipred* predictions, the largest metal-binding protein group identified in the *M. pusilla* proteome were proteins associated with Zn. A further 21 Zn-binding proteins were identified based on GO annotation. The relative abundance of Zn-binding proteins showed an average decline in response to warming, from 3.2 % to 2.8 %, however this decline was not statistically significant ($p = 0.10$). Sixty-five Zn-proteins were identified to display altered abundance in the warmed treatment (q ≤ 0.05) (Supplementary data Table 3). The Zn-proteins displaying a greatest increase (*i.e.* >1.00 FC) were primarily annotated as predicted proteins. One of these proteins was identified using the Zn-ion binding GO term only, the remaining three were identified as Zn-binding by *mebipred*, however in each case binding was predicted for several additional ions. In addition, a protein-serine/threonine kinase (C1MI13) was recorded to display a 1.02 FC increase under warming (q ≤ 0.05) (Fig. 4). This protein's annotation had no metal-binding associated GO terms and was only predicted to bind Zn by *mebipred*. Seven Zn-proteins were recorded to display a decline of −1.00 FC or below in the warmed treatment (Supplementary data Table 3). This included both Mg-protoporphyrin IX chelatase (C1MUK3) and Mg chelatase (C1MQ15) involved in chlorophyll biosynthesis and typically associated with Mg [57]. A calcineurin-like phosphoesterase (C1MJS2) displayed a − 1.51 FC decline, whilst adenosylhomocysteinase (C1MNU4) was reduced −1.10 FC (q ≤ 0.05). Both of these proteins were predicted to also bind Ni. The latter, plays a role in the activated methyl cycle and binds NAD as a cofactor [58], hence its down-regulation may be related to the decline in Fe-binding quinolinate synthase described above.

3.3.4. Magnesium & manganese

Approximately half of the Mg-binding proteins identified in the *M. pusilla* proteome displayed significantly altered abundance under warming conditions (Supplementary data Table 3). A key role of Mg in photosynthetic organisms is its incorporation into chlorophyll. The greatest alteration of any Mg-binding protein was that of Mg chelatase (C1MQ15), displaying a − 1.90 FC decline in the warmed treatment (q ≤ 0.05) (Fig. 4). A further three Mg-proteins involved in the chlorophyll biosynthetic pathway were identified to be significantly reduced −0.80 to −1.20 FC in the warmed treatment (q ≤ 0.05). Other notable alterations in the Mg-binding group included a − 1.40 FC decline in pyruvate kinase (C1MYX6) under warming (q ≤ 0.05) (Fig. 4). Such a result may indicate an alteration in glycolytic activity, however, a further two proteins annotated as pyruvate kinase (C1MK78 and C1MT92) displayed a significant 0.58–0.94 FC increase under warming (q ≤ 0.05). Whilst pyruvate kinase is known to bind Mg^{2+} [59], *mebipred* also predicted this protein to bind Mn. The Mn-binding D-fructose-1,6-bisphosphate 1-phosphohydrolase (C1N730), also involved in carbon metabolism displayed a 1.07 FC increase in the warmed treatment (q ≤ 0.05) (Fig. 4). The final notable alteration in Mn-binding protein abundance was that of the light induced-like protein (C1N3F9) which displayed a − 1.33 FC decline compared to the control (q ≤ 0.05) (Fig. 4). These proteins are reported to be similar to light-harvesting proteins [60,61], thus their reduction in abundance may be correlated to the reduction in photosynthetic proteins observed under warming.

3.3.5. Nickel, cobalt & copper

A total of 52 Ni-binding proteins were included proteomic analysis, 19 of which displayed altered abundance in the warmed treatment relative to the control (q ≤ 0.05) (Supplementary data Table 3). All but three of these proteins were predicted to bind >1 ion. Little functional insight could be gained from those Ni-binding proteins displaying

greatest variation under warming. Ten Cu-binding proteins were found to be significantly altered by increasing temperature (q ≤ 0.05). Here, just one protein displayed a FC >1. This predicted protein (C1MHV2) was predicted to bind an additional four ligands (Co, K, Mn and Zn). Notable alterations in Cu-protein abundance was that of 1,4-alpha-glucan branching enzyme (C1MXZ5) and alpha-1,4 glucan phosphory-lase (C1N0C2), which were significantly raised (0.55 FC) and reduced (−0.93 FC) in response to warming, respectively (q ≤ 0.05). These two enzymes play roles in glycogen synthesis and catabolism; respectively, hence their altered abundance appears to suggest an increase in glycogen storage in *M. pusilla* under warming, which alongside reductions in ribosomal content and increased protein synthesis will likely influence the C:N:P ratio of *M. pusilla* in a warmed ocean. Little difference was observed in abundance of Co-binding proteins.

3.4. Changing demand for trace metals in M. pusilla under ocean warming?

Proteomic analysis reveals a clear impact of temperature upon metalloprotein abundance, thus likely driving altered regulation of metal homeostasis and cofactor synthesis within the cell. Tools such as *mebipred* expand our capacity to explore changing cellular demand for metals by identifying those proteins most likely to interact with metal ions. However, difficulty arises when a protein is found to bind more than one metal, to resolve this, additional characterisation and analysis would be required to confirm the exact metal bound. Some of the greatest changes are recorded in proteins not identified by *mebipred*, highlighting the importance of using a combined approach of metal-binding prediction and use of existing annotation as presented in this study.

The total relative abundance of specific metal-binding protein groups showed negligible variation between control and warmed treatments, suggesting an unaltered cellular demand for the ion in question. It is possible that overall cell metal quotas remain relatively constant given the wide-ranging roles which metalloproteins play in the cell, as various functions are up- and down-regulated in response to the environment. The consistency observed in relative abundance of metal-binding proteins under warming in *M. pusilla* may also be species- or lineage- specific. Indeed, genomics studies on *Micromonas* have revealed greater defence against heavy metals than related *Ostreococcus* [62], likely enhancing metal homeostasis. Previous work has shown that the elemental stoichiometry of green algae is relatively stable, even when exposed to high levels of Cr [63]. This work on *Chlamydomonas concordia* suggested that the green lineage algae are well-equipped to control their intracellular metal quota [63], hence under environmental change such as ocean warming the metal quota of green algae may show little change. It would be of great interest to examine whether phytoplankton belonging to the red superfamily displays a greater variation in metalloprotein abundance. The *mebipred* tool provides scope to carry out such work in species where reference proteomes are available.

A limitation of using the relative abundance of metalloproteins to gain insight towards impacts on cellular stoichiometry is the lack of consideration of the elemental composition of the metalloprotein of interest. This may also play a part in the perceived stability of trace metal composition in *M. pusilla* described in this study. The clearest example of this is the respective Fe content of PSI and PSII. PSI contains 12 Fe ions, whilst PSII typically contains 2–3 Fe ions [64–66], hence, an increase in PSI protein abundance may have a greater impact on the cellular Fe quota than increases in PSII. Such methods have been used to examine changes in phytoplankton Fe stoichiometry in previous research [67]. However, this is dependent on detailed understanding of metalloprotein structure and elemental composition, which is currently limited. One limitation of *mebipred* is therefore its inability to predict the number of ion binding sites for each metal, advancements in predictive tools in this area would be highly beneficial. In this study both PSI and PSII appeared down-regulated under warming, suggestive of a decrease

in cellular Fe content. However, this coincided with a significant increase in ferritin abundance, likely responding to the reduced photosynthetic Fe demand [14]. The apparent storage of Fe by ferritin at higher temperature suggests that Fe limitation is unlikely. However, this increase may be required to support elevated levels of heme production and Fe—S cluster assembly observed. Alternatively, this increase in ferritin may display a shuttling between Fe storage and use as environmental conditions change. Previously, ferritin has been shown to play a key role in the day-night cycling of Fe in the green alga, *Ostreococcus* [49]. The increase in ferritin, therefore, may represent a transition from Fe use to storage as temperatures rise. In this manner the overall cellular Fe quota likely remains relatively unchanged, in-line with observations of total Fe-binding protein abundance. As the ocean warms, increased oligotrophy is predicted to occur due to stratification of the water column [34], reducing the supply of essential nutrients such as Fe to surface layers. Should increases in temperature reduce investment in photosynthetic machinery due to improved photosynthetic efficiency [33], this may alleviate some of the cellular demand for Fe, in doing so mitigating the adverse effect of any reduction in Fe supply. Such an effect is only likely to occur if temperature increases are within the sub-optimal to optimal thermal range for growth. Past the thermal optima, where rates of photosynthesis rapidly decline [13], reduced Fe supply may significantly hamper algal growth, particularly as Fe limits algal growth in much of the open ocean [9]. Additional work is required to resolve whether cellular metal quotas are relatively stable, but the proportion of metal which shuttles between use and storage is largely controlled by environmental conditions.

A number of the key proteomic alterations observed were related to metals that are in plentiful supply in seawater, likely having limited impact on growth of *M. pusilla*. For example, a clear down-regulation of chlorophyll biosynthesis was observed, reducing demand for a number of Mg-binding proteins, thus reducing cellular Mg demand. In contrast a number of Ca-binding proteins were shown to increase in abundance under warming, potentially increasing cellular Ca requirement. Whilst Ca is freely available in seawater, any increase in active transport into the cell such as that of Ca-transporting ATPase recorded to display a 1.36 FC increase under warming, comes at an energetic cost to the cell.

It should be noted that this study was conducted under nutrient replete conditions and results are likely to be greatly altered if the experiment was repeated under nutrient limitation. Indeed, nutrient availability is reported to influence phytoplankton growth to a greater extent than temperature [68]. The stability in relative abundance of metal-binding groups above may arise due to trace metals being freely available in replete media, hence mitigating any disadvantageous effect of warming on metalloprotein abundance as luxury uptake and storage of trace metals may occur [1]. It is possible that the storage of Fe by ferritin observed in our study represents luxury Fe storage under the replete conditions used. Additional experimentation would be highly beneficial to explore changes in metalloprotein abundance under combined exposure to nutrient limitation and warming given that both processes will likely occur simultaneously in the modern ocean. This is of particular interest given that our findings add to the growing consensus that phytoplankton N:P will rise under warming due to an increase in translation efficiency [12,32,33,69], likely enhancing N limitation in areas where concentrations of this major element is scarce and as the surface ocean becomes increasingly stratified [70].

4. Conclusions

Acclimation to warming conditions caused several major alterations to the cellular function in *M. pusilla*, including; reduced ribosomal investment, increased protein synthesis and transport, and a down-regulation of chlorophyll synthesis and photosynthetic machinery. If common across various phytoplankton taxa, these changes will likely influence cellular C:N:P ratios in the future ocean, impacting local and global biogeochemical cycles. Associated with alterations in cellular

function, 47 % of metalloproteins identified using *mebipred* and GO terms were recorded to display significantly altered abundance under warming. A consideration of individual protein stoichiometry is required to accurately calculate the proteomic metal quota, however examination of relative abundance of metal-binding protein groups suggests that the metal quota of *M. pusilla* will be little affected by warming, further demonstrating the ability of green algae to effectively manage metal homeostasis. Notably, under experimental conditions warming appears to cause a decline in photosynthetic Fe demand in *M. pusilla* and increase abundance of the Fe-storage protein, ferritin.

Ocean warming inevitably drives altered requirements for metalloproteins within the cell and hence impacts cellular demand and regulation of metal cofactors. To investigate this further, additional experimentation under nutrient limitation and on additional species would be beneficial. Extending studies to include community-wide responses will be key in understanding the overall impact of warming on the marine environment. Despite the limitations discussed, tools such as *mebipred* offer great scope to enhance annotation of reference proteomes and facilitate analysis of altering metalloprotein abundance from shotgun proteomic data. In this study we have outlined how such tools may be applied to assess how demand for metalloproteins alters under an environmental perturbation such as ocean warming.

Supplementary data to this article can be found online at https://doi.org/10.1016/j.algal.2024.103412.

CRediT authorship contribution statement

Craig J. Dedman: Writing – review & editing, Writing – original draft, Visualization, Investigation, Formal analysis, Conceptualization. **Marjorie Fournier:** Writing – review & editing, Resources, Methodology, Investigation. **Rosalind E.M. Rickaby:** Writing – review & editing, Supervision, Funding acquisition, Conceptualization.

Declaration of competing interest

The authors declare that they have no known competing financial interests or personal relationships that could have appeared to influence the work reported in this paper.

Data availability

Data will be made available on request.

Acknowledgements

References

[1] W.G. Sunda, Feedback interactions between trace metal nutrients and phytoplankton in the ocean, Front. Microbiol. 3 (2012) 204.
[2] F.M. Morel, The co-evolution of phytoplankton and trace element cycles in the oceans, Geobiology 6 (3) (2008) 318–324.
[3] Q. Zhang, E.M. Bendif, Y. Zhou, B. Nevado, R. Shafiee, R.E.M. Rickaby, Declining metal availability in the Mesozoic seawater reflected in phytoplankton succession, Nat. Geosci. 15 (2022) 932–941.
[4] K.J. Waldron, J.C. Rutherford, D. Ford, N.J. Robinson, Metalloproteins and metal sensing, Nature 460 (7257) (2009) 823–830.
[5] UniProt UniProt, The universal protein knowledgebase in 2021, Nucleic Acids Res. 49 (D1) (2021) D480–D489.
[6] C. UniProt, UniProt: a worldwide hub of protein knowledge, Nucleic Acids Res. 47 (D1) (2019) D506–D515.
[7] A.A. Aptekmann, J. Buongiorno, D. Giovannelli, M. Glamoclija, D.U. Ferreiro, Y. Bromberg, Mebipred: identifying metal binding potential in protein sequence, Bioinformatics 38 (14) (2022) 3532–3540.
[8] D.A. Hutchins, C.E. Hare, R.S. Weaver, Y. Zhang, G.F. Firme, G.R. Di Tullio, M. B. Alm, S.F. Riseman, J.M. Maucher, M.E. Geesey, C.G. Trick, G.J. Smith, E.L. Rue,

J. Conn, K.W. Bruland, Phytoplankton iron limitation in the Humboldt current and Peru upwelling, Limnol. Oceanogr. 47 (2002) 997–1011.
[9] J.K. Moore, S.C. Doney, D.M. Glover, I.Y. Fung, Iron cycling and nutrient-limitation patterns in surface waters of the World Ocean, Deep Sea Res. II (49) (2002) 463–507.
[10] P.W. Boyd, T. Jickells, C.S. Law, S. Blain, E.A. Boyle, K.O. Buesseler, K.H. Coale, J. J. Cullen, H.J. de Baar, M. Follows, M. Harvey, C. Lancelot, M. Levasseur, N. P. Owens, R. Pollard, R.B. Rivkin, J. Sarmiento, V. Schoemann, V. Smetacek, S. Takeda, A. Tsuda, S. Turner, A.J. Watson, Mesoscale iron enrichment experiments 1993-2005: synthesis and future directions, Science 315 (5812) (2007) 612–617.
[11] IPCC, Summary Report for Policymakers. In: Global Warming of 1.5 °C, IPCC, Geneva, Switzerland, 2018.
[12] A. Toseland, S.J. Davies, J.R. Clark, A. Kirkham, J. Strauss, C. Uhlig, T.M. Lenton, K. Valentin, G.A. Pearson, V. Moulton, T. Mock, The impact of temperature on marine phytoplankton resource allocation and metabolism, Nature Clim Change 3 (11) (2013) 979–984.
[13] S. Barton, J. Jenkins, A. Buckling, C.E. Schaum, N. Smirnoff, J.A. Raven, G. Yvon-Durocher, Evolutionary temperature compensation of carbon fixation in marine phytoplankton, Ecol. Lett. 23 (4) (2020) 722–733.
[14] I. Yruela, Transition metals in plant photosynthesis, Metallomics 5 (9) (2013) 1090–1109.
[15] S. Barton, G. Yvon-Durocher, Quantifying the temperature dependence of growth rate in marine phytoplankton within and across species, Limnol. Oceanogr. 64 (5) (2019) 2081–2091.
[16] K.G. Baker, R.J. Geider, Phytoplankton mortality in a changing thermal seascape, Glob. Chang. Biol. 27 (20) (2021) 5253–5261.
[17] M.K. Thomas, C.T. Kremer, C.A. Klausmeier, E. Litchman, A global pattern of thermal adaptation in marine phytoplankton, Science 338 (6110) (2012) 1085–1088.
[18] Y. Zhang, J. Zheng, Bioinformatics of Metalloproteins and Metalloproteomes, Molecules 25 (2020) 15.
[19] H.M. Berman, J. Westbrook, Z. Feng, G. Gilliland, T.N. Bhat, H. Weissig, I. N. Shindyalov, P.E. Bourne, The Protein Data Bank, Nucleic Acids Res. 28 (1) (2000) 235–242.
[20] A.Z. Worden, F. Not, Microbial Ecology of the Oceans, Wiley, Hoboken, NJ, 2008.
[21] D. Demory, A.C. Baudoux, A. Monier, N. Simon, C. Six, P. Ge, F. Rigaut-Jalabert, D. Marie, A. Sciandra, O. Bernard, S. Rabouille, Picoeukaryotes of the Micromonas genus: sentinels of a warming ocean, ISME J. 13 (1) (2019) 132–146.
[22] D.W. Huang, B.T. Sherman, R.A. Lempicki, Systematic and integrative analysis of large gene lists using DAVID bioinformatics resources, Nature Protoc. 4 (1) (2009) 44–57.
[23] B.T. Sherman, M. Hao, J. Qiu, X. Jiao, M.W. Baseler, H.C. Lane, T. Imamichi, W. Chang, DAVID: a web server for functional enrichment analysis and functional annotation of gene lists (2021 update), Nucleic Acids Res. 50 (W1) (2022) W216–W221.
[24] Guillard, R. R. L.; Ryther, J. H.; , Studies of marine planktonic diatoms. I. Cyclotella nana Hustedt and Detonula confervaceae (Cleve) Gran. *Can. J. Microbiol.* 1962, 8, 229–239.
[25] M.M. Bradford, A rapid and sensitive method for the quantitation of microgram quantities of protein utilizing the principle of protein-dye binding, Anal. Biochem. 72 (1976) 248–254.
[26] J. Cox, M. Mann, MaxQuant enables high peptide identification rates, individualized p.p.b.-range mass accuracies and proteome-wide protein quantification, Nat. Biotechnol. 26 (12) (2008) 1367–1372.
[27] J. Cox, M.Y. Hein, C.A. Luber, I. Paron, N. Nagaraj, M. Mann, Accurate proteome-wide label-free quantification by delayed normalization and maximal peptide ratio extraction, termed MaxLFQ *Mol*, Cell Proteom. 19 (9) (2014) 2513–2526.
[28] S. Tyanova, T. Temu, P. Sinitcyn, A. Carlson, M.Y. Hein, T. Geiger, M. Mann, J. Cox, The Perseus computational platform for comprehensive analysis of (prote) omics data, Nat. Methods 13 (9) (2016) 731–740.
[29] A. Kaur, J.R. Hernandez-Fernaud, M.D.M. Aguilo-Ferretjans, E.M. Wellington, J. A. Christie-Oleza, 100 days of marine Synechococcus-Ruegeria pomeroyi interaction: a detailed analysis of the exoproteome, Environ. Microbiol. 20 (2) (2018) 785–799.
[30] The Gene Ontology, C, The gene Ontology resource: 20 years and still GOing strong, Nucleic Acids Res. 47 (D1) (2019) D330–D338.
[31] Y. Perez-Riverol, J. Bai, C. Bandla, D. Garcia-Seisdedos, S. Hewapathirana, S. Kamatchinathan, D.J. Kundu, A. Prakash, A. Frericks-Zipper, M. Eisenacher, M. Walzer, S. Wang, A. Brazma, J.A. Vizcaino, The PRIDE database resources in 2022: a hub for mass spectrometry-based proteomics evidences, Nucleic Acids Res. 50 (D1) (2022) D543–D552.
[32] D. Varkey, S. Mazard, M. Ostrowski, S.G. Tetu, P. Haynes, I.T. Paulsen, Effects of low temperature on tropical and temperate isolates of marine Synechococcus, ISME J. 10 (5) (2016) 1252–1263.
[33] C.J. Dedman, S. Barton, M. Fournier, R.E.M. Rickaby, The cellular response to ocean warming in Emiliania huxleyi, Front. Microbiol. 14 (2023) 1177349.
[34] N. Gruber, Warming up, turning sour, losing breath: ocean biogeochemistry under global change, Philos Trans A Math Phys Eng Sci 2011 (369) (1943) 1980–1996.
[35] C.M. Moore, M.M. Mills, K.R. Arrigo, I. Berman-Frank, L. Bopp, P.W. Boyd, E. D. Galbraith, R.J. Geider, C. Guieu, S.L. Jaccard, T.D. Jickells, J. La Roche, T. M. Lenton, N.M. Mahowald, E. Marañón, I. Marinov, J.K. Moore, T. Nakatsuka, A. Oschlies, M.A. Saito, T.F. Thingstad, A. Tsuda, O. Ulloa, Processes and patterns of oceanic nutrient limitation, Nat. Geosci. 6 (9) (2013) 701–710.
[36] L. Kwiatkowski, O. Aumont, L. Bopp, P. Ciais, The impact of variable phytoplankton stoichiometry on projections of primary production, food quality,

and carbon uptake in the Global Ocean, Global Biogeochem. Cycles 32 (4) (2018) 516–528.

[37] C. Lovejoy, W.F. Vincent, S. Bonilla, S. Roy, M.-J. Martineau, R. Terrado, M. Potvin, R. Massana, C. Pedrós-Alió, DISTRIBUTION, PHYLOGENY, AND GROWTH OF COLD-ADAPTED PICOPRASINOPHYTES IN ARCTIC SEAS1, J. Phycol. 43 (1) (2007) 78–89.

[38] H.K. Ahn, J.T. Yoon, I. Choi, S. Kim, H.S. Lee, H.S. Pai, Functional characterization of chaperonin containing T-complex polypeptide-1 and its conserved and novel substrates in Arabidopsis, J. Exp. Bot. 70 (10) (2019) 2741–2757.

[39] T. Hunter, Prolyl isomerases and nuclear function, Cell 92 (2) (1998) 141–143.

[40] Bednar, J.; Horowitz, R. A.; Grigoryev, s. A.; Carruthers, l. m.; Hansen, J. C.; Koster, A. J.; Woodcock, C. L., Nucleosomes, linker DNA, and linker histone form a unique structural motif that directs the higher-order folding and compaction of chromatin. PNAS 1998, 95 (24), 14173–14178.

[41] T. Kawashima, Z.J. Lorkovic, R. Nishihama, K. Ishizaki, E. Axelsson, R. Yelagandula, T. Kohchi, F. Berger, Diversification of histone H2A variants during plant evolution, Trends Plant Sci. 20 (7) (2015) 419–425.

[42] A. Veluchamy, A. Rastogi, X. Lin, B. Lombard, O. Murik, Y. Thomas, F. Dingli, M. Rivarola, S. Ott, X. Liu, Y. Sun, P.D. Rabinowicz, J. McCarthy, A.E. Allen, D. Loew, C. Bowler, L. Tirichine, An integrative analysis of post-translational histone modifications in the marine diatom Phaeodactylum tricornutum, Genome Biol. 16 (2015) 102.

[43] R.B. Deal, S. Henikoff, Histone variants and modifications in plant gene regulation, Curr. Opin. Plant Biol. 14 (2) (2011) 116–122.

[44] M.N. Fodje, A. Hansson, J.G. Olsen, S. Gough, R.D. Willows, A. Al-Karadaghi, Interplay between an AAA module and an integrin I domain may regulate the function of magnesium chelatase, J. Mol. Biol. 311 (1) (2001) 111–122.

[45] L.-M. Cheng, S.-F. Zhang, Z.-X. Xie, D.-X. Li, L. Lin, M.-H. Wang, D.-Z. Wang, Metabolic adaptation of a globally important diatom following 700 generations of selection under a warmer temperature, Environ. Sci. Technol. 56 (2022) 5247–5255.

[46] S. Thangaraj, J. Sun, Transcriptomic reprogramming of the oceanic diatom Skeletonema dohrnii under warming ocean and acidification, Environ. Microbiol. 23 (2) (2021) 980–995.

[47] S.I. Allakhverdiev, V.D. Kreslavski, V.V. Klimov, D.A. Los, R. Carpentier, P. Mohanty, Heat stress: an overview of molecular responses in photosynthesis, Photosynth. Res. 98 (1–3) (2008) 541–550.

[48] J.A. Raven, R.J. Geider, Temperature and algal growth, New Phytol. 110 (1988) 441–461.

[49] H. Botebol, E. Lesuisse, R. Sutak, C. Six, J.C. Lozano, P. Schatt, V. Verge, A. Kirilovsky, J. Morrissey, T. Leger, J.M. Camadro, A. Gueneugues, C. Bowler, S. Blain, F.Y. Bouget, Central role for ferritin in the day/night regulation of iron homeostasis in marine phytoplankton, Proc. Natl. Acad. Sci. U. S. A. 112 (47) (2015) 14652–14657.

[50] O.T. Jones, Haem synthesis by isolated chloroplasts, Biochem. Biophys. Res. Commun. 28 (5) (1967) 671–674.

[51] B.B. Buchanan, Regulation of CO2 assimilation in oxygenic photosynthesis: the ferredoxin/thioredoxin system. Perspective on its discovery, present status, and future development, Arch. Biochem. Biophys. 288 (1) (1991) 1–9.

[52] H. Sakuraba, H. Tsuge, K. Yoneda, N. Katunuma, T. Ohshima, Crystal structure of the NAD biosynthetic enzyme quinolinate synthase, J. Biol. Chem. 280 (29) (2005) 26645–26648.

[53] A. Lewit-Bentley, S. Rety, EF-hand calcium-binding proteins, Curr. Opin. Struct. Biol. 10 (6) (2000) 637–643.

[54] M. Michalak, E.F. Corbett, N. Mesaeli, K. Nakamura, M. Opas, Calreticulin: one protein, one gene, many functions, Biochem. J. 344 (2) (1999) 281–292.

[55] R.E. Zielinski, Calmodulin and calmodulin-binding proteins in plants, Annu. Rev. Plant. Physiol. Plant. Mol. Biol. 49 (1998) 697–725.

[56] Q. Wang, S. Yang, S. Wan, X. Li, The significance of calcium in photosynthesis, Int. J. Mol. Sci. 20 (6) (2019).

[57] S.I. Beale, Enzymes of chlorophyll biosynthesis, Photosynth. Res. 60 (1999) 43–73.

[58] M.A. Turner, X. Yang, D. Yin, K. Kuczera, R.T. Borchardt, P.L. Howell, Structure and function of S-adenosylhomocysteine hydrolase, Cell Biochem. Biophys. 33 (2) (2000) 101–125.

[59] T.J. Bollenbach, T. Nowak, Kinetic linked-function analysis of the multiligand interactions on mg(2+)-activated yeast pyruvate kinase, Biochemistry 40 (43) (2001) 13097–13106.

[60] S. Jansson, A guide to the Lhc genes and their relatives in Arabidopsis, Trends Plant Sci. 4 (6) (1999) 236–240.

[61] J.A. Neilson, D.G. Durnford, Evolutionary distribution of light-harvesting complex-like proteins in photosynthetic eukaryotes, Genome 53 (1) (2010) 68–78.

[62] A.Z. Worden, J.H. Lee, T. Mock, P. Rouze, M.P. Simmons, A.L. Aerts, A.E. Allen, M. L. Cuvelier, E. Derelle, M.V. Everett, E. Foulon, J. Grimwood, H. Gundlach, B. Henrissat, C. Napoli, S.M. McDonald, M.S. Parker, S. Rombauts, A. Salamov, P. Von Dassow, J.H. Badger, P.M. Coutinho, E. Demir, I. Dubchak, C. Gentemann, W. Eikrem, J.E. Gready, U. John, W. Lanier, E.A. Lindquist, S. Lucas, K.F. Mayer, H. Moreau, F. Not, R. Otillar, O. Panaud, J. Pangilinan, I. Paulsen, B. Piegu, A. Poliakov, S. Robbens, J. Schmutz, E. Toulza, T. Wyss, A. Zelensky, K. Zhou, E. V. Armbrust, D. Bhattacharya, U.W. Goodenough, Y. Van de Peer, I.V. Grigoriev, Green evolution and dynamic adaptations revealed by genomes of the marine picoeukaryotes Micromonas, Science 324 (5924) (2009) 268–272.

[63] W. Wilson, Q. Zhang, R.E.M. Rickaby, Susceptibility of algae to Cr toxicity reveals contrasting metal management strategies, Limnol. Oceanogr. 64 (5) (2019) 2271–2282.

[64] J.A. Raven, Predictions of Mn and Fe use efficiencies of phototrophic growth as a function of light availability for growth and C assimilation pathway, New Phytol. 116 (1990) 1–18.

[65] R.F. Strzepek, P.J. Harrison, Photosynthetic architecture differs in coastal and oceanic diatoms, Nature 431 (7009) (2004) 689–692.

[66] W.G. Sunda, S.A. Huntsman, High iron requirement for growth, photosynthesis, and low-light acclimation in the coastal cyanobacterium Synechococcus bacillaris, Front. Microbiol. 6 (2015) 561.

[67] J.T. Snow, D. Polyviou, P. Skipp, N.A. Chrismas, A. Hitchcock, R. Geider, C. M. Moore, T.S. Bibby, Quantifying integrated proteomic responses to Iron stress in the globally important marine Diazotroph Trichodesmium, PLoS One 10 (11) (2015) e0142626.

[68] E. Maranon, P. Cermeno, M. Huete-Ortega, D.C. Lopez-Sandoval, B. Mourino-Carballido, T. Rodriguez-Ramos, Resource supply overrides temperature as a controlling factor of marine phytoplankton growth, PLoS One 9 (6) (2014) e99312.

[69] T. Tanioka, K. Matsumoto, A meta-analysis on environmental drivers of marine phytoplankton C : N : P, Biogeosciences 17 (2020) 2939–2954.

[70] K. Matsumoto, T. Tanioka, R.E.M. Rickaby, Linkages Between Dynamic Phytoplankton C:N:P and the Ocean Carbon Cycle Under Climate Change, Oceanography 33 (2) (2020) 44–52.